https://doi.org/10.56801/MME889

Air and Vacuum Annealing Effect on the Highly Conducting and Transparent Properties of the Undoped Zinc Oxide Thin Films Prepared by DC Magnetron Sputtering

Lamia Radjehi[1,2], Linda Aissani[2,3], Abdelkader Djelloul[1,2], Abdenour Saoudi[4], Salim Lamri[5], Komla Nomenyo[6], Gilles Lerondel[6], Frédéric Sanchette[5,7]

[1]*LASPI2A Laboratoire des Structures, Propriétés et Interactions Inter Atomiques, Khenchela University, Khenchela 40000, Algeria*
[2]*Matter Sciences Department, Abbes Laghrour-Khenchela University, P.O 1252, 40004 Khenchela, Algeria*
[3]*Active Components and Materials Laboratory, Larbi BEN M'HIDI University, 04000 Oum El Bouaghi, Algeria*
[4]*Department of Mechanical Engineering, and Advanced Materials Laboratory (ISMA), Abbes Laghrour University, Khenchela 40000, Algeria*
[5]*Laboratoire des Systèmes Mécaniques et d'Ingénierie Simultanée, Institut Charles Delaunay, CNRS, Université de Technologie de Troyes (UTT), Antenne de Nogent, Pôle technologique de Haute-Champagne, 52800 Nogent, France*
[6]*Light, Nanomaterials, Nanotechnologies (L2N, former LNIO), Institut Charles Delaunay, CNRS, Université de Technologie de Troyes (UTT), 12 Rue Marie Curie, CS 42060, 10004 Troyes, France*
[7]*Nogent International Center for CVD Innovation, LRC CEA-ICD LASMIS, UTT, Antenne de Nogent-52, Pôle Technologique de Haute-Champagne, 52800 Nogent, France*

Received: 27-08-2022
Accepted: 31-03-2023

Abstract: In this study, we aim to investigate the effect of zinc interstitials (Zni) and oxygen vacancies (VO) on the ZnO electrical conductivity. ZnO films were synthesized via DC magnetron sputtering process using pure Zn target in gases mixture of Ar/O_2 = 80/17.5 sccm. In order to improve the optical and electrical prosperities, the obtained films were subjected to air and vacuum annealing treatment. Several techniques such as field emission scanning electron microscopy (FESEM), Grazing Incidence X-ray Diffraction (GIXRD), Raman spectroscopy, photoluminescence spectroscopy (PL) and UV-visible were used to study the influence of heat treatment on ZnO properties. Electrical conductivity of ZnO films was determined by measuring the sheet resistance and thickness of the films. As deposited and under vacuum annealing films showed a lower electrical resistivity of 2.72×10^{-3} and 1.17×10^{-2} Ωcm, respectively, due to the Zn-rich conditions. ZnO films under air treatment show a intensity decrease of (103) plane and an optical transmittance of 87 %.

Keywords: Vacuum annealing; ZnO; Zni; VO; optical transmittance; electrical resistivity.

*Corresponding authors: Abdenour Saoudi, saoudiabdenour@gmail.com

1. Introduction

Zinc oxide is one of the promising materials used in wide range applications due to its exceptional optical and electronic properties [1]. It is a material of high potential in solar cells, organic light emitting diodes, photocatalysis of organic compounds and gas sensors [2-4]. Furthermore, ZnO films are used in the modern electrical and optical systems and for products having low resistivity and transmittance performances [5]. Electrical resistivity depends on different factors such as crystal defects and heat treatment. ZnO thin films deposited on glass substrates have several defects, which include zinc vacancies (VZn), oxygen vacancies (VO), oxygen interstitials (Oi), zinc interstitials (Zni), or their combinations [6]. The donor type of VO and Zni defects with lowest formation energy are created under zinc-rich conditions. Conversely, under oxygen-rich conditions, the most favorable defects are acceptor type: zinc vacancies VZn, interstitial oxygen Oi. These defects can provide universal guidelines for understanding the electrical properties of transparent thin films.

The control of donors or acceptors defects type has attracted the attention of researchers towards the use of this material in the electro-optical field (e.g. solar cells, electro-optical and sensors) [1-3]. D. Kim et al, [7] found that the large number of oxygen vacancies in the ZnO with low formation energy is a main source of free electrons. Zni was also proposed as another source of free electrons in the conduction band with high formation energy [8].

Though, the number and the types of defects largely vary and depend on the deposition method and process parameters, one among them, annealing treatment is one important factor that affect the defects. The thermal treatment of ZnO in an O-poor ambient leads to the formation of Zn-interstitials (Zni) and O-vacancies (VO). Zni' (single charged), Zni" (doubly charged), and ZniX (neutral) are shallow donors with an energy level located below the bottom of the conduction band (CB). Similar to Zni, VO also exists in neutral (VOX), single (VO'), and doubly charged states (VO"), which are deep donors with energy levels located below the minimum conduction Band (CB).

After heat treatment, ZnO films have shown remarkable improvements in optical quality and chemical stability and low resistivity as compared to other films [9-13]. Few researchers studied the dependence of annealing treatment with crystalline defects and succeeded in explaining the VO and Zni contribution in electrical conductivity of ZnO films. A. R. Hutson [14] found that after annealing the change of defect level in the crystal depends to the annealing atmosphere. Other hind, Oxygen vacancies present a potential contribution on the n-type conductivity of ZnO. Some reports indicate that the increase of substrate temperature in the 200–250 °C range enhance the crystallite size and decrease the electrical resistivity. But, at higher temperature, the electrical resistivity clearly increased owing to the decrease of the electrical mobility [15; 16]. Furthermore, annealing vacuum presents an effective improvement of the grain size, concentration and mobility of charges of ZnO films [9], conversely to the annealing treatment under oxygen atmospheres [10].

However, in the literature there have been insufficient investigations on the combination of the structural, optical and electrical properties of sputtered ZnO films (composition, band gap and conductivity) after air and vacuum annealing [11]. The evolution of the microstructure and optical properties at different annealing temperature, or the influence of vacancies and Zni concentration were discussed without understanding the evolution of electrical resistivity as function of heat treatment [12; 17].

In this work, ZnO films with low resistivity were deposited via the magnetron cathode sputtering method. It is possible to optimize deposit conditions of ZnO film rich in zinc which favorite the formation of ZnO rich in interstitial zinc. The influence of air and vacuum annealing on structural, electrical and optical properties of ZnO thin films was investigated.

A deep explanation of the relationship between vacuum annealing and film structure will be presented to select the ZnO film with good transmittance and low resistivity. This will

contribute to understand the ZnO defect responsible for electrical conduction in films, in particular Zni and VO. This work provides required data about the structure and phase formation of the films, transmittance, as well as resistivity for choosing optimal factors for the best improvement of opto-electrical properties of ZnO films.

2. Experimental procedure

ZnO films were deposited using DC magnetron sputtering system (Plassys MP-450, 13.56 MHz, 3 kW). High purity Zn (99.99 % purity and 100×200×6 mm^3) rectangular target was used. The substrates-target distance was fixed at 80 mm and with an angle of 90° from the normal to obtain films with uniform thickness and good deposition rate. Films were deposited on Si (100) wafers (20××10×0.38 mm^3) and glass (26763 mm^3) substrates. The coated Si wafers were used to measure the chemical composition, film thickness and surface morphology. Whereas, the coated glass substrates were used to evaluate the structural, optical and electrical properties. Thereafter, the substrates were cleaned in an ultrasonic bath of acetone and ethanol solution for 10 min and then dried by air. Prior to the deposition procedure, the chamber was evacuated dawn to a low pressure of 1×10^{-5} Pa. The substrates and targets were cleaned by Ar ion etching for 10 min, to remove the oxides and other adherent impurities. The cleaning step was performed with the following conditions: argon flow rate of 210 sccm, pressure of 0.7 Pa, voltage of 450 V applied to Zn target. ZnO thin films were deposited for 10 min at a temperature of 68 °C, working pressure of 0.78 Pa. The current density and the applied power were kept constant at 0.934 A/cm^2 and 619 W, respectively. The film deposition was carried out in a mixture atmosphere (Ar and O_2) with partial pressure of 80 sccm of Ar and 17.5 sccm of O_2.

Then, ZnO films were annealed under vacuum and air atmosphere at 450 °C in a tubular furnace. The thermal cycle consisted in a ramp of 10 °C/min, followed by maintaining at the desired temperature for 1 hour. Finally, the cooling takes place under vacuum at a rate of about 10 °C/min. A diffusion pump insured the pressure of 10^{-7} Pa. The crystallographic structures of films were analyzed by Grazing incidence X-ray diffraction (GIXRD, Panalyatical B.V., X'Pert) using Cu-Kα radiation (λ=1.54 Å, 40 kV, 40 mA). A θ-2θ scan was carried out for 2θ diffraction angles ranging from 20 to 80° with a scan step of 0.02°. The crystallite size was determined using the Scherrer's formula:

$$D = \frac{0.94\lambda}{\beta\cos\theta} \quad (1)$$

By using the Bragg equation [2]:

$$d_{hkl} = \frac{\lambda}{2\sin\theta_{hkl}} \quad (2)$$

Where θ is the angle between the normal of the diffracting plane and the incident X-ray, λ is the wavelength of the X-ray. In our case CuKα = 1.5405 Å, and n is the order of the diffracted beam.

The lattice parameters of ZnO thin films were calculated using Miller indices (h k l) according the formula for the hexagonal following the equation:

$$\frac{1}{d_{hkl}^2} = \frac{4}{3a^2}(h^2 + hk + k^2) + \frac{l^2}{c^2} \quad (3)$$

Where h, k and l are the Miller indices, and a = b and c are the parameters of the mesh along the x, y, and z directions. Since we are concerned with the directions (002) and (100) of ZnO, then h = 0, k = 0 and l = 2 and h = 1, k = 0.

The surface morphology and the elemental chemical composition of films were measured by using a scanning electron microscopy (FEG-SEM, Hitachi, SU-8030) and Energy Dispersive X-ray Spectroscopy (EDS Bruker), respectively. Raman measurements were

recorded with a Labram HR 800 (HORIBA JobinYvon) spectrometer. The photoluminescence (PL) measurements were carried out at room temperature by using the 325 nm line of He–Cd laser as the excitation source. The film thickness (d) was determined by fitting experimental transmittance data by using optical habbal program [18]. The optical transmission of ZnO films was observed in the wavelength range of 200 and 2500 nm using spectrometer (UV-3101PC UV-Vis scanning spectrophotometer Shimadzu).

In the Drude theory, ωp is expressed by:

$$\omega_p = \frac{2\pi c}{\lambda_p} = \left(\frac{e^2 N_{opt}}{m^* \varepsilon_\infty \varepsilon_0}\right)^{1/2} \quad (4)$$

In this equation: ω_p, e, N_{opt}, and ε_0 are the plasma angular frequency, electron charge, optical carrier concentration, and free-space permittivity, respectively.

The electron effective mass in ZnO $m^*=0.24m_0$ and $\varepsilon_\infty=n_\infty^2$

Electrical proprieties were characterized by four points at room temperature using a Keithley Source Measure Unit. The resistivity (ρ) was calculated by the following eq:

$$\rho = R_{sq} \times d \quad (5)$$

Where (d) is the film thickness and (Rsq) id the sheet resistance.

3. Results and discussion

3.1. Structure and microstructure

The energy dispersive X-ray (EDS) spectra and the chemical composition of ZnO films before and after annealing treatment are shown in Figure 2. The crystal model was established, with the lattice parameter set as follows: a=b=3.249Å; c=5.207Å; α=β=90°; γ=120°. Based on the construction and optimization of primitive cells, the supercells were constructed and then optimized. Figure 1 presents the ZnO lattice with Zni and VO. Zni atoms are occupied the oxygen interstitial positions in the ZnO hexagonal system.

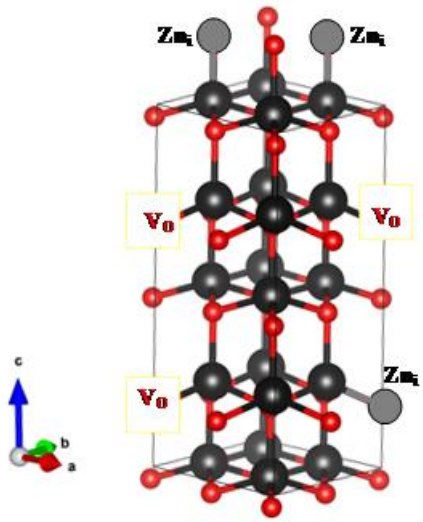

Figure. 1. *Schematic presentation of ZnO bulk with Zni and Vo defects.*

The EDS spectra confirm the presence of Zn (1, 8.6, and 9.6 keV) and O peak (0.8 keV). In addition, Si signal is detected from the glass substrate in the EDS spectra due to the low ZnO

film thickness as compared by a large EDS interaction volume. The quantitative analysis of the as deposited ZnO film is 60.3 % Zn and 39.7 at. % O, which indicates the under stoichiometric between Zn and O atoms with O/Zn ratio of 0.66. This suggest that the presence of Zni in the octahedral sites, as seen in Figure 1. After vacuum annealing, we noticed a decrease of oxygen from 39.7 down to 34.4 at. % with O/Zn ratio of about 0.52, due to reduction of oxygen in the heat environment [16]. However, the Zn/O ratio is increased and ZnO film becomes stoichiometric (O/Zn ~ 1) with increasing of oxygen from 39 to 48.4 at. %. Therefore, the chart in Fig. 2(C) shows that the Zn decreased due to the oxygen insertion in the Zn lattice and the formation of ZnO phase. R. Ghosh et al, [19] explained the high oxygen amount by the relative oxidation of ZnO film during the air annealing. As deposited ZnO film exhibits a dense morphology formed by small nano-wire grain stack to shape a columnar-type structure with 672 nm of film thickness (Fig. 2. A). The average roughness and the crystallite size are about (40 nm, 22.6 nm). After air annealing, the ZnO film seems a dense and rough surface with not very well-defined globular grains. It is characterized by the presence of voids between grains, due to relatively high atoms mobility and execs film by oxygen after annealing treatment (Fig. 2 B) [17; 19]. However, after vacuum annealing, ZnO film shows a smooth and dense surface, thus the grain size was obviously decreased with an elongated sharp (Fig. 2 C). Through measured, the average roughness and the crystallite size are about the (44 nm, 26.6 nm), and (46 nm, 28.4 nm) for ZnO films after air and vacuum annealing, respectively (Table 1). ZnO surface roughness increases due to the agglomeration and coalescence of the grains. These results indicate that the structure of the ZnO film has significantly changed after oxygen diffusing into ZnO film by increasing Zn-O bond and decreasing Zn-Zn bond. After annealing temperature lead to the increase of grain size of the based ZnO thin films prepared by reactive magnetron sputtering, thus the improvement of crystalline quality as annealing supplies sufficient energy for atom rearrangement [20]. According to D. Shiwen et al, [21] the grain refinement of ZnO film after vacuum annealing is due to the dislocation in the larger grain boundaries associated with low grain size that influence the restriction in the grains movement. So, the large grain with smooth surface can influence the different properties [22].

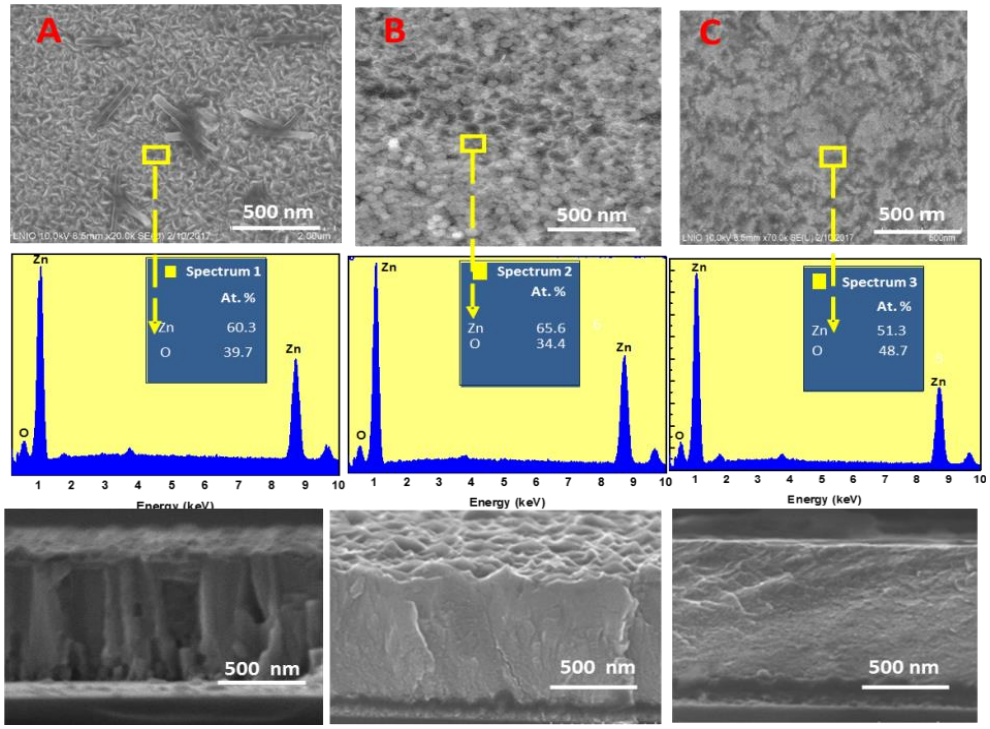

Figure. 2. *SEM cross-sections and surface images of the ZnO films: A) as deposited, B) after air annealing, C) after vacuum annealing.*

Figure 3 shows GRXD patterns of ZnO films before and after annealing in air and vacuum. Before annealing, the diffraction pattern presents strong (002) and (103) peaks at 34.42° and 62.86 ° and minors (100), (101), (102) and (112), at 31.77°, 36.25°, 47.53° and 67.96° peaks of the hexagonal ZnO phase (JCPDS file (36-1451). Similar results have also been observed by Y. Wang et al, [23] which induced that the origin of the low dense (103) diffraction might be related to the under stoichiometric of the based ZnO film. The lattice parameter of ZnO phase of the as deposited ZnO film is about (aZnO = 3.2618 Å, cZnO = 5.1986 Å). This value is close to that obtained in JCPDS file (36-1451) of the bulk ZnO phase, (aZnO(bulk) = 3.2498 Å, cZnO(bulk) = 5.2066 Å) with high lattice strain ($\varepsilon = 0.0252$) due to the distortion of the ZnO lattice by the insertion of Zn atoms as shown in Figure 4. After vacuum annealing, we noticed a slight decrease in the (103) peak intensity and the disappearance of minors (100), (101), (102) and (112) peaks. However, ZnO film shows a high intensity of (002) plane along c-axis as compared to (103) and a decrease the lattice parameters of ZnO phase down to (aZnO = 3.2198 Å, cZnO = 5.1903 Å) after air annealing. The decrease of (103) peak and the increase of (200) is due to distortion of ZnO lattice with the oxidation and saturation by oxygen by the rearrangement of ZnO crystalline structure [20; 22; 24]. However, after vacuum annealing, the ZnO film shows a remarkable decrease in both oxygen content (34.5 %) and the lattice parameter of ZnO phase at bout (aZnO = 3.1798 Å, cZnO = 5.1839 Å). This is due to the loss of oxygen at the film surface that is subsequent increase in oxygen vacancies [25]. Figure 4 presents the presentation of (002) and (103) in the ZnO lattice.

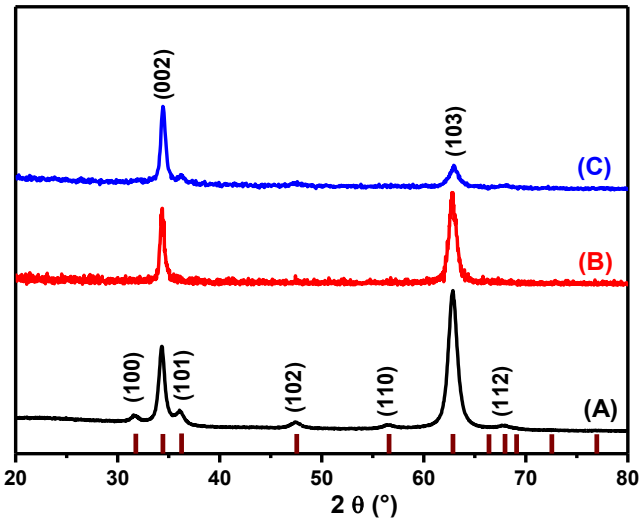

Figure. 3. *GIXRD patterns of ZnO films: A) as deposited, B) after vacuum annealing, C) after air annealing.*

The plan presentation was visualized using, with the lattice parameter set as follows: a = b = 3.249 Å; c = 5.207 Å; $\alpha = \beta = 90°$; $\gamma = 120°$. Based on the construction and optimization of primitive cells, the supercells were constructed and then optimized. Finally, (002) and (103) planes were cut and the planar supercell structure was constructed. In order to make a plane representation for the solid bulk with 10 Å of thickness.

Grains with (002) orientation have the low surface energy 9.9 eV nm^{-2} and a high density, as compared by (103) as seen in Figure 4. After air annealing, the ZnO Thin film has a low defects concentration, which causes crystal lattice relaxation and promotes the (002) preferred orientation due to deformation energy minimization. Grains with (002) orientation grow in the normal direction to the film plane, which contributes to the formation of a columnar microstructure, while (103) grains grow in the normal inclined direction, having the potential to change the columnar morphology as presented in Figure 2.

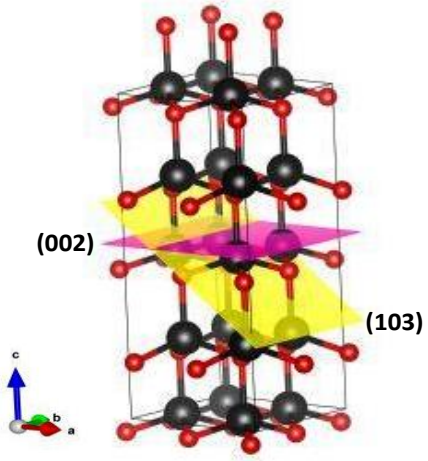

Figure. 4. *Schematic presentation of (002) and (103) planes on the bulk ZnO crystal.*

Through the Scherrer equation, the crystallite size of the hexagonal crystalline ZnO phase was calculated and the values obtained are summarized in Table 1. The results indicate that the crystalline size of ZnO phase increased from 22.6 to 28.4 nm with a low strain (ε = 0.0132). after annealing. Recent studies of sputtered ZnO films are in line with these observations especially grain coalescence by heat treatment [26].

Table 1. *Structural properties of ZnO films before and after air and vacuum annealing treatment.*

ZnO Samples	Film thickness (nm)	(O)/(Zn)	Film strain (ε)	S. roughness (nm)	Grain size (nm)
As deposited	680	0.52	0.0252	44	22.6
Vacuum annealing	650	0.64	0.0202	40	26.6
Air annealing	590	0.94	0.0132	46	28.4

In order to compare the evolution of structural modifications before and after annealing treatment of ZnO films, the Raman spectroscopy was performed on the films. The Raman spectra are presented in Figure 5. For the two films, before and after vacuum annealing, we can identify strong and large bands centered at 560 cm^{-1} with other minor peaks at 98, 276, 430, and 850 cm^{-1} it associated with ZnO phase [27]. The ZnO band located at 560 cm^{-1} was larger and more intense indicating finer grain size for these films [26].The enlargement of these peaks is due to the low compressive stress generated in the films, which is in agreement with Zn-O bonds detected by Raman analysis in the sputtered ZnO film [28]. Moreover, a slight shift between 560 and 567 cm^{-1} was observed for the film annealed in vacuum as compared to as deposited film [29]. This suggests that O atoms occupy the interstitial sites of Zn crystal structure, which can be attributed to the oxide character of the Zn-O bonds. S. B. Yahia, et al, [30] have reported a similar behavior in the ZnO films, suggesting that the predominant (002) ZnO structure forms with oxygen inserted through the system ZnO. The scattering peak at 560 and 1080 cm^{-1} is attributed to the quartz ZnO. It is clear that the typical Raman E2 (high) mode of ZnO appears at about 430 cm^{-1} for as deposited and vacuum annealed samples, indicating that all films have the characteristic of the wurtzite phase [31]. However, after air annealing; a notable decrease in their intensity can be observed. The intensity of the ZnO bands is very lower than that of the vacuum annealed film, suggesting that formation of amorphous ZnO and the

exec of O atoms occupy all vacancies of ZnO crystal structure. In other hand, up on annealing in air, zinc in the film becomes oxidized, the impurity states disappear, and the magnitude of resonance Raman enhancement of the E, (LO) mode is diminished. S. B. Yahia, et al, [30] has found unchanged with weak Raman peaks in the sputtered ZnO films annealed in air.

We find from the structural study that the heating and cooling rate of 10 °C/min gives time for solidification and recrystallization of thin films and to have dense ZnO films that leads to improving their properties.

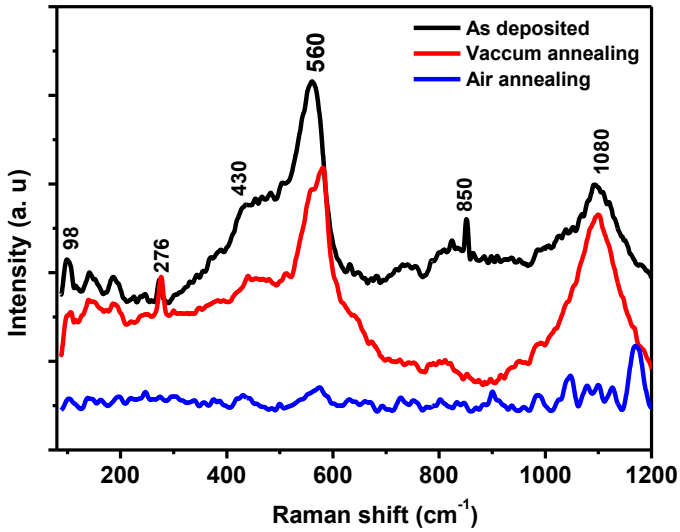

Figure. 5. *Raman spectra of ZnO films before and after annealing: A) as deposited, B) after vacuum annealing, C) after air annealing.*

Figure 6 shows the transmittance in the UV-VIS regions of the deposited ZnO films before and after heat treatment in the wavelength range of 200-2500 nm together with the corresponding simulated curves. All samples present a large absorption in the UV region and a good transparency in the visible wavelength range and the absorption edge is around 375 nm for all the films. The simulated curves are shown as the solid lines inside the symbol curve that represent experimental data. The Figures reveal a good fitting to the experimental data, implying the accurate determination of the parameters, which are presented in reference [32].

It can be seen that the transmittance of ZnO film is about 68 %, which is comparable to most of the previous studies [26]. The ZnO transmittance was improved after heat treatment as compared to that of the as deposited ZnO film. The enhancement in transmittance is attributed to the effect of grain refinement and solid solution transpiring of ZnO phase, which was also observed in previous studies [10; 19]. V. Gokulakrishnan et al, [33], found that the transmittance of GZO film is 84% in the visible region (400–800 nm) with the transmission edge shift towards the shorter-wavelength side on annealing.

Moreover, the transmittance enhancement from 68 to 87 % was observed for air annealing ZnO film, due to oxygen insertion in Zn-O system and a disappearance of VO and Zni in the ZnO lattice. According to Y. Hu et al, [34] the annealing in air at high temperature may remove some defects reducing thus the defect scattering and then increasing the transmittance.

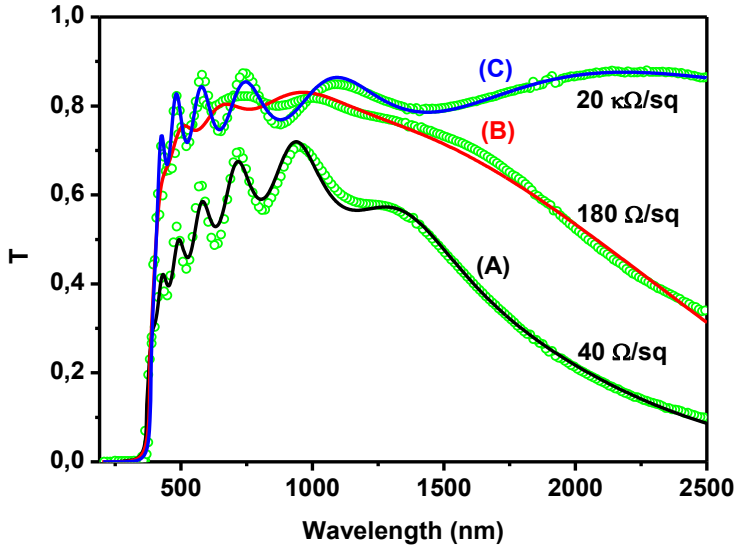

Figure. 6. *Optical transmittance spectra for ZnO films: A) as deposited, B) after vacuum annealing, C) after air annealing.*

The optical values extracted by fitting the experimental data with MATLAB software [32] are listed in Table 2. The optical energy band-gap of the as deposited ZnO film was estimated at 3.36 eV. This value is slightly near to the bulk ZnO phase value of 3.31 eV [35] and in good agreement with previously reported data of deposited ZnO thin films [8]. After air annealing, a noticeable red shift of the absorption edges can be observed. The value of the direct optical band-gap is decreased from 3.36 to 3.24 eV. V. Gokulakrishnan et al, explained the change in the optical band gap by the Burstein–Moss shift, since the absorption edge of a degenerate semiconductor is shifted slightly toward shorter wavelengths with increasing carrier concentration by Ga doping and annealing [33]. In our case, the same shift has been observed and is accompanied with an increase in the sheet resistivity from 40 Ω/sq to a value of 20 KΩ/sq (Fig. 6). However, a remarkable decrease in the optical energy band-gap down to 3.22 eV, after vacuum annealing, with decreasing oxygen count due to decrease of the oxygen content.

Table 2. *Dispersion parameters of the Zn films extracted by fitting the experimental data.*

ZnO film	Thickness (nm)	Eg (eV)	n at 598 nm	n_∞	λ_p (nm)	$N_{opt}\times10^{20}$ cm^{-3}	ρ (Ωcm)
As-deposited	667	3.36	2.15	2.07	1352	6.27	2.72×10^{-3}
Vacuum annealing	590	3.24	1.67	1.61	1705	2.38	1.17×10^{-2}
Air annealing	593	3.22	1.93	1.79			1.18

Figure 7 presents the calculated refractive index of ZnO film before and after (air and vacuum annealing) versus wavelength. For all films, the relationship between the refractive index and the wavelength exhibits the same tendency. At 598 nm, the refractive index of the as deposited ZnO is about 2.15, which is higher than that of bulk ZnO [19].

Furthermore, it is found that the refractive indices below the band gap gradually decreased after annealing treatment of the ZnO film to 1.93 and 1.67, respectively, (at 598 nm), owing to the reduction of absorption-related defects during the preferred growth of the stable (002) ZnO film (Fig. 4). This indicated that the stable (002) ZnO film predominantly grown

had fewer Zni and VO crystal defects than the (002) and (103) mixed ZnO film, leading to a decrease in the deep level emission after annealing treatment.

In photovoltaic cells, the ZnO n-type semiconductor with a band gap of 3.3 eV is a good absorbent of UV light and is a good transmitter of visible light. This light passes to the absorbing thin films (p-type semiconductor), this makes it possible to generate electricity in the optical devices.

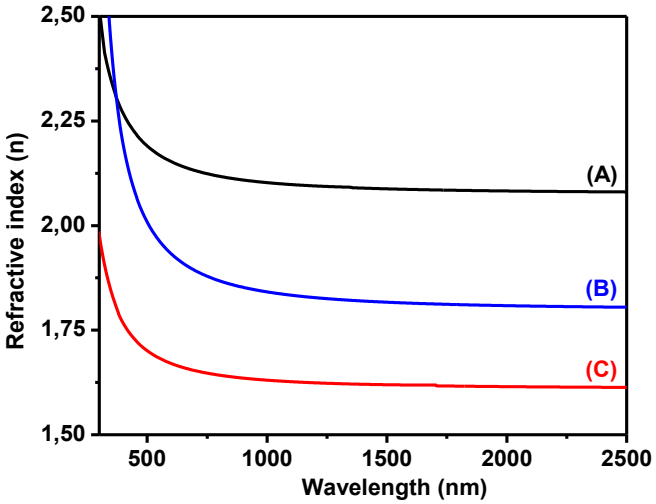

Figure. 7. *Band gap of ZnO films: A) as deposited, B) after vacuum annealing, C) after air annealing.*

The typical PL spectra of the as-deposited and annealed ZnO films are illustrated in Figure 7. The broad PL bands are deconvoluted with Gaussian fit due to the overlap of many bands that are attributed to the existence of different deep energy bands. There are a visible luminescence ranging from 2.70-1.60 eV (470-530 nm). ZnO has a wide band gap of 3.31 eV with the corresponding wavelength of about 375 nm. A violet peak located at 402 nm (3.08 eV) presents a broad and asymmetric band of the as deposited and vacuum annealing films suggesting the well crystallized ZnO film [36]. This peak gives information on the recombination in the near band edge (NBE) of ZnO and electronic decay from CB to energy deep defects band corresponds to the NBE emission the make the recombination of the free exactions of ZnO [37; 38].

In air annealing, the violet peak was shifted toward the lower energy values from 3.08 to 3.01 eV with a clear decrease in their intensity due to the high lattice strain ($\varepsilon = 0.0132$) [39]. In the visible range, the fitted emission bands have the same shape and intensities as compared to as deposited and vacuum annealing ZnO films: orangered regions (1.7 eV), yellow (2.05) green (2.16 and 2.23 eV), and blue emission (2.7 eV). R. N. Aljawf et al, [40] rapport that ZnO films revealed green, orange, or red emission due to transition of the photoexcited electrons from the CB (conduction band) to VO, Zni or from the CB to the mid-gap states, respectively. However, air annealed ZnO film presents weak peaks with low intensities (Fig 8). While, no deep level (DL) emission bands were observed in the PL spectrum, as shown in Figure 6. this is due to the well crystallinity and reducing of the Vo^{2+} point defect. Furthermore, they observed the disappearance of deep PL bands that attributed to Zni by the insertion of oxygen on the vacancies position of ZnO crystal, shown in eqs (5, 6):

$$V_0 + \frac{1}{2} O_2 = O_o \tag{6}$$

$$Zn_i + \frac{1}{2} O_2 = Zn_{Zn} + O_o = ZnO \tag{7}$$

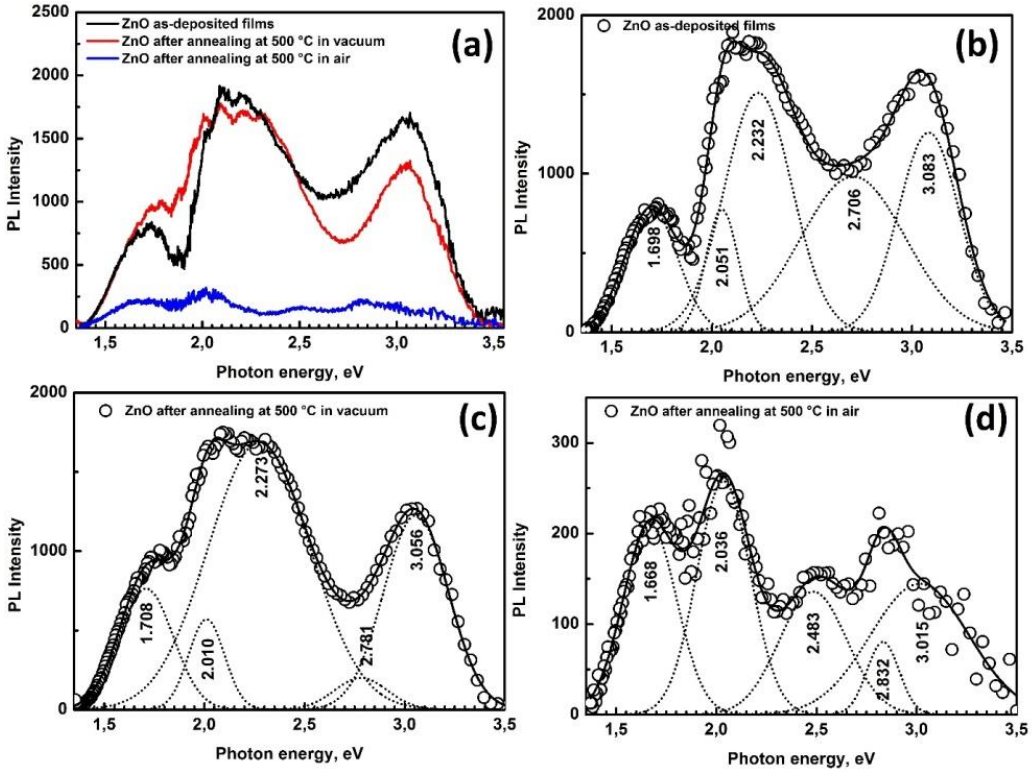

Figure. 8. *PL spectra of ZnO films a) before and after heating in b) as-deposited c) after vacuum annealing d) after air annealing.*

In order to study electrical proprieties of ZnO thin films, the resistance was measured by four-point method, as shown in Table 2.

Vacuum and air annealing is holding at the desired temperature for 1 hour, which is done in ovens with thermocouples that ensure the same temperature during thermal treatment. To maintain the homogeneous temperature, ZnO features a thermal conductivity as high as 60 W m^{-1} K^{-1} that can be lowered. In addition, the as deposited film shows the resistivity value of 40 Ω/sq that indicate good conductivity with calculated charge carrier 6.27×1020 cm^{-3}. Vacuum annealing led to small increase in sheet resistivity value (180 Ω/sq) and calculated charge carrier (2.38×1020 cm^{-3}) due to effects diminution. However, after air annealing the ZnO film has a highest sheet resistivity of 20 KΩ/sq due to dense structure and the disappearance of defects with oxygen insertion.

In order to evaluate the stability of resistivity of ZnO film during heat treatment, the electrical in-situ measurement has been performed as function as temperature (Fig. 9). The heating rate was set to 2 °C/min and the films temperature was maintained at 500 °C for one hour, and then it was gradually lowered to room temperature as it shown in Figure 9, the resistivity value remains stable between 25 and 370 °C at about 40 Ω/sq. From 370 °C, the resistivity gradually increased at 2.72×10^{-3} Ωcm, ZnO films due to the air oxidation. Similar results were observed in previous studies, that described the resistance increase of AZO and ZnO films as a function of temperature by the oxygen chemisorptions that is a native defect donor such as VO and Zni [41; 42].

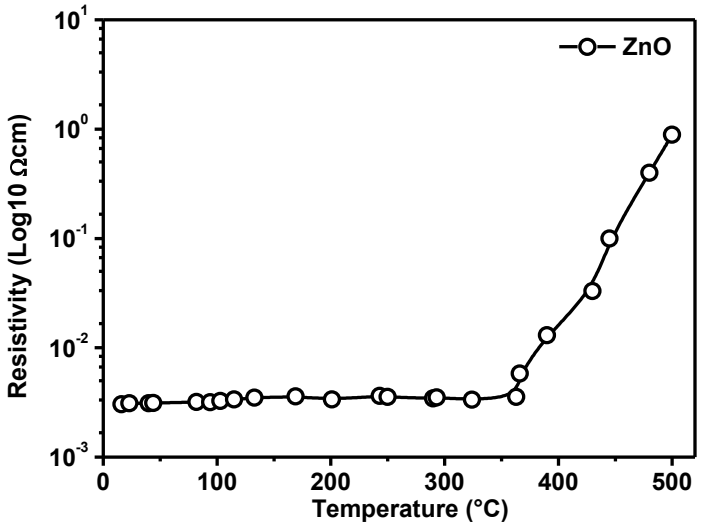

Figure. 9. *Resistivity as function as temperature in-situ for ZnO heated in air.*

4. Conclusions

Un-doped ZnO thin films with high conductive, high transparency and smooth surface morphology were synthesized on glass and Si wafer substrate using DC magnetron sputtering. We investigated the effect of the heat treatment on the crystallographic and optical properties of ZnO thin films. XRD results reveal that the as-deposited ZnO films have hexagonal structure with (103) predominant direction. XRD results confirm the synthesis of annealed ZnO films of the hexagonal structure with a preferential orientation along the (002) plane. The average crystallite size is altered between 22.6 to 28.4 nm dependent on the plan orientation of the ZnO film. Raman scattering reveals that the 560 cm^{-1} peak and the shoulder peaks (98, 276, 430, and 850 cm^{-1}) originate from ZnO. After annealing the film morphology become dense with a further increase in the (200) plan intensity. The good optical band gap of about 3.36 eV was obtained for as deposited ZnO film. The difference in the transmittance value can be explained by difference in the oxygen mount, which influences optical properties of the ZnO film.

Morphology and crystallinity of the ZnO structure could efficiently control the transmittance, electrical resistivity and optical band gap. PL spectra of ZnO films at room temperature show that the intensity of visible emission reduces. This is due to the decrease of the number of the oxygen vacancies and/or Zn interstitials in the films. Based on these results, we believe that the annealed ZnO films with (103) preferential orientation presents a low resistivity of 40 Ω/sq.

ZnO films developed in this study with high transmittance and low resistivity and good electro-optical quality supports their use in transparent and conductive electrode applications.

References

[1] Shelke, V., Bhole, M., & Patil, D. (2012). Open air annealing effect on the electrical and optical properties of tin doped ZnO nanostructure. *Solid state sciences*, *14*(6), 705-710.

[2] Manivasaham, A., Ravichandran, K., & Subha, K. (2017). Light intensity effects on the sensitivity of ZnO: Cr gas sensor. *Surface Engineering*, *33*(11), 866-876.

[3] Radjehi, L., Djelloul, A., Lamri, S., Slim, M. F., & Rahim, M. (2019). Oxygen effect on structural and optical properties of zinc oxide. *Surface Engineering*, *35*(6), 520-526.

[4] Oh, S., & Kim, J. (2019). Correlation between the Morphology of ZnO Layers and the Electroluminescence of Quantum Dot Light-Emitting Diodes. *Applied Sciences*, *9*(21), 4539.

[5] Cai, P., You, J., Zhang, X., Dong, J., Yang, X., Yin, Z., & Chen, N. (2009). Enhancement of conductivity and transmittance of ZnO films by post hydrogen plasma treatment. *Journal of Applied Physics*, *105*(8), 083713.

[6] Janotti, A., & Van de Walle, C. G. (2007). Native point defects in ZnO. *Physical Review B*, *76*(16), 165202.

[7] Kim, D.-H., Lee, G.-W., & Kim, Y.-C. (2012). Interaction of zinc interstitial with oxygen vacancy in zinc oxide: An origin of n-type doping. *Solid state communications*, *152*(18), 1711-1714.

[8] Ahn, C. H., Kim, Y. Y., Kim, D. C., Mohanta, S. K., & Cho, H. K. (2009). A comparative analysis of deep level emission in ZnO layers deposited by various methods. *Journal of Applied Physics*, *105*(1), 013502.

[9] Li, J., Huang, J.-H., Zhang, Y.-L., Yang, Y., Song, W.-J., & Li, X.-M. (2011). Effects of rapid thermal annealing in different ambients on structural, electrical, and optical properties of ZnO thin films by sol-gel method. *Journal of electroceramics*, *26*, 84-89.

[10] Benramache, S., Chabane, F., Benhaoua, B., & Lemmadi, F. Z. (2013). Influence of growth time on crystalline structure, conductivity and optical properties of ZnO thin films. *Journal of Semiconductors*, *34*(2), 023001.

[11] Tsuji, T., & Hirohashi, M. (2000). Influence of oxygen partial pressure on transparency and conductivity of RF sputtered Al-doped ZnO thin films. *Applied Surface Science*, *157*(1-2), 47-51.

[12] Mathew, J. P., Varghese, G., & Mathew, J. (2014). Structural and optical properties of Ni: ZnO thin films-effect of annealing and doping concentration. *Sop Trans. Appl. Phys*, *1*, 27-36.

[13] Hoggas, K., Nouveau, C., Djelloul, A., & Bououdina, M. (2015). Structural, microstructural, and optical properties of Zn 1− x Mg x O thin films grown onto glass substrate by ultrasonic spray pyrolysis. *Applied Physics A*, *120*, 745-755.

[14] Hutson, A. R. (1957). Hall effect studies of doped zinc oxide single crystals. *Physical review*, *108*(2), 222.

[15] Li, W., Sun, Y., Wang, Y., Cai, H., Liu, F., & He, Q. (2007). Effects of substrate temperature on the properties of facing-target sputtered Al-doped ZnO films. *Solar Energy Materials and Solar Cells*, *91*(8), 659-663.

[16] Minami, T. (2008). Present status of transparent conducting oxide thin-film development for Indium-Tin-Oxide (ITO) substitutes. *Thin Solid Films*, *516*(17), 5822-5828.

[17] K.E. Knutsen, A. Galeckas, A. Zubiaga, F. Tuomisto, G. C. Farlow, B. G. Svensson, A. Y. Kuznetsov: Physical Review B, 86 (2012) 121-203.

[18] Ellmer, K. (2000). Magnetron sputtering of transparent conductive zinc oxide: relation between the sputtering parameters and the electronic properties. *Journal of Physics D: Applied Physics*, *33*(4), R17.

[19] Ghosh, R., Paul, G., & Basak, D. (2005). Effect of thermal annealing treatment on structural, electrical and optical properties of transparent sol–gel ZnO thin films. *Materials research bulletin*, *40*(11), 1905-1914.

[20] Li, L., Liang, F., Ximing, C., Gaobin, L., Jun, L., Fengfan, Y., . . . Chunyang, K. (2007). Effect of annealing treatment on the structural, optical, and electrical properties of Al-doped ZnO thin films. *Rare Metals*, *26*(3), 247-253.

[21] D. Shiwen, L. Yongtang: Advances in Materials Science and Engineering, 5 (2015) 1-8.

[22] Water, W., & Chu, S.-Y. (2002). Physical and structural properties of ZnO sputtered films. *Materials Letters*, *55*(1-2), 67-72.

[23] Wang, Y., Li, X., Jiang, G., Liu, W., & Zhu, C. (2013). Origin of (103) plane of ZnO films deposited by RF magnetron sputtering. *Journal of Materials Science: Materials in Electronics*, *24*, 3764-3767.

[24] Usseinov, A., Kotomin, E., Akilbekov, A., Zhukovskii, Y. F., & Purans, J. (2014). Hydrogen induced metallization of ZnO ($1\bar{1}00$) surface: Ab initio study. *Thin Solid Films*, *553*, 38-42.
[25] Tu, Y., Chen, S., Li, X., Gorbaciova, J., Gillin, W. P., Krause, S., & Briscoe, J. (2018). Control of oxygen vacancies in ZnO nanorods by annealing and their influence on ZnO/PEDOT: PSS diode behaviour. *Journal of Materials Chemistry C*, *6*(7), 1815-1821.
[26] S. Yang. Y. Liu. Y. Zhang, D. Mo: Bulletin of Materials Science, 33 (2014) 209-214.
[27] Sharma, S., & Exarhos, G. (1997). Raman spectroscopic investigation of ZnO and doped ZnO films, nanoparticles and bulk material at ambient and high pressures. Solid State Phenomena,
[28] Lee, J.-H., Oh, K., Jung, K., Wilson, K., & Lee, M.-J. (2020). Tuning the morphology and properties of nanostructured Cu-ZnO thin films using a two-step sputtering technique. *Metals*, *10*(4), 437.
[29] Zhang, P., Kong, C., Li, W., Qin, G., Xu, Q., Zhang, H., . . . Fang, L. (2015). The origin of the∼ 274 cm− 1 additional Raman mode induced by the incorporation of N dopants and a feasible route to achieve p-type ZnO: N thin films. *Applied Surface Science*, *327*, 154-158.
[30] Yahia, S. B., Znaidi, L., Kanaev, A., & Petitet, J. (2008). Raman study of oriented ZnO thin films deposited by sol–gel method. *Spectrochimica Acta Part A: Molecular and Biomolecular Spectroscopy*, *71*(4), 1234-1238.
[31] K. Elmer, R. Mientus: Solid State Phenomena, 37-38 (1994) 433.
[32] Roguai, S., Djelloul, A., Nouveau, C., Souier, T., Dakhel, A., & Bououdina, M. (2014). Structure, microstructure and determination of optical constants from transmittance data of co-doped Zn0. 90Co0. 05M0. 05O (MAl, Cu, Cd, Na) films. *Journal of alloys and compounds*, *599*, 150-158.
[33] V. Gokulakrishnan, V. Purushothaman, E. Arthi, K. Jeganathan, K. Ramamurth: The physica status solidi (pss) journal, 209 (2012) 1-6.
[34] Hu, Y., Diao, X., Wang, C., Hao, W., & Wang, T. (2004). Effects of heat treatment on properties of ITO films prepared by rf magnetron sputtering. *Vacuum*, *75*(2), 183-188.
[35] A. A. Alnajjar: Advances in Condensed Matter Physics, 8 (2012) 682125.
[36] Xiu, F., Yang, Z., Mandalapu, L., Zhao, D., & Liu, J. (2005). Photoluminescence study of Sb-doped p-type ZnO films by molecular-beam epitaxy. *Applied Physics Letters*, *87*(25), 252102.
[37] Ghosh, J., Ghosh, R., & Giri, P. (2018). Tuning the visible photoluminescence in Al doped ZnO thin film and its application in label-free glucose detection. *Sensors and Actuators B: Chemical*, *254*, 681-689.
[38] Giri, P., Bhattacharyya, S., Singh, D. K., Kesavamoorthy, R., Panigrahi, B., & Nair, K. (2007). Correlation between microstructure and optical properties of ZnO nanoparticles synthesized by ball milling. *Journal of Applied Physics*, *102*(9), 093515.
[39] Aissani, L., Fellah, M., Radjehi, L., Nouveau, C., Montagne, A., & Alhussein, A. (2019). Effect of annealing treatment on the microstructure, mechanical and tribological properties of chromium carbonitride coatings. *Surface and Coatings Technology*, *359*, 403-413.
[40] Aljawf, R. N., Rahman, F., & Kumar, S. (2016). Defects/vacancies engineering and ferromagnetic behavior in pure ZnO and ZnO doped with Co nanoparticles. *Materials research bulletin*, *83*, 108-115.
[41] Minami, T., Nanto, H., & Takata, S. (1984). Highly conductive and transparent aluminum doped zinc oxide thin films prepared by RF magnetron sputtering. *Japanese Journal of Applied Physics*, *23*(5A), L280.
[42] S. Y. Ma, X. H. Yang, X. L. Huang, A. M. Sun, H. S. Song, H. B. Zhu: Journal of Alloys and Compounds, 45 (2013) 9-15. .